Mechanical Stability and Flow Analysis of Hollow Microneedle Array for Transdermal Drug Delivery

Gowthami Anbazhagan[1], Sreeja B S[1]
1. Department of Electronics and Communication Engineering,Anna University,Chennai,TN,India.

Abstract

Two different geometry structures such as conical and pyramidal hollow microneedle were taken into consideration for the drug delivery. A detailed analysis of geometry optimization is performed with the specification of microneedle height (400-1000 μm), base diameter (150-300 μm), tip diameter (10-30 μm) and center-to-center spacing of 650 μm. The microneedle array is made with PVA material and comprises of 16 microneedles arranged in 4x4 matrix. With the use of solid mechanics module, a stress analysis is conducted on 4x4 conical and pyramidal microneedle array under axial and bending loading conditions. The impact of modification of microneedle geometry with respect to mechanical stability was examined. An in-depth flow analysis is performed with laminar flow module, in which water and glucose were used as the fluids for the microfluidic study. It has been discovered that sharper conical tip has greater mechanical stability with less bending and a higher flow rate of 320 μL/min compared to a pyramidal microneedle array, which has a flow rate of 230 μL/min. The skin insertion finite element analysis of 4x4 PVA microneedle array is performed with three layer skin model and the endurance of the microneedle array is examined by applying a buckling load to the microneedle base which results in less stress and bending.

Keywords: Hollow Microneedle,Transdermal Drug Delivery,Geometry.

Introduction

Microneedles(MN) are micron size needles of less than 1mm in length especially used for efficient transdermal drug delivery (Mccrudden *et al.*, 2013)(Ita, 2015).The finite element analysis (FEA) has received a great deal of interest recently in the MN sector (Yan *et al.*, 2022). The analysis helps to avoid expensive experimental trials and provides the pathway to create customized MN according to patient skin. All the previous works of hollow microneedle are analysed with single microneedle of different geometry with single or double side opened lumen or centred lumen(Griss and Stemme, 2002)(Wang *et al.*, 2009)(Ranamukhaarachchi *et al.*, 2016).Hollow SU-8 microneedles were created by Mishra et al. in a straightforward and effective manner (Mishra, Maiti and Bhattacharyya, 2018). The cylindrical body of a microneedle with a sharp tip were sufficient to puncture skin quickly and effectively. Kanakaraj et al (Sawon and Samad, 2021) introduced an out-of-plane microneedle with six lumens for drug passage. COMSOL software was used to perform the structural analysis on silicon carbide material. The work investigates the fluidic analysis utilizing various viscosity-based fluids and examines the structural mechanics of the microneedle. In another study, an investigation of the stress and flow analysis of cylindrical microneedles with a side-open lumen is performed. The experiment used PGA (polyglycolide as structural material (Bodhale, Nisar and Afzulpurkar, 2010). The microneedles are constructed with copper and silver material and ANSYS software is used to analyze the stress effect and deformation on the single microneedle (Tariq *et al.*, 2022).

The detailed finite element analysis such as stress and fluidic analysis of biocompatible hollow microneedle for transdermal drug delivery is studied. A conical and pyramidal hollow microneedle array with centered open holes is proposed to confirm drug distribution after skin insertion. A built-in drug reservoir is also included in the present design and is located on the back of the microneedle array.

This is the first new attempt for the mechanical and fluidic analysis of conical and pyramidal microneedle array. There are no studies that have been published on the hollow-centered PVA microneedle array with an integrated reservoir to forecast mechanical and fluid flow characteristics under different criteria. Certain additional factors, such as pressure, fluid velocity and flow rate, must be considered while designing the microneedle for drug administration (Mcallister, Allen and R, 2000).The size and position of the lumen also plays a crucial role to get the desired flow rate (Bodhale, Nisar and Afzulpurkar, 2010). The present study elaborately discuss on the effect of geometry parameters in relation to stress and flow analysis. The geometry structure also dependent on the flow rate of the drug, here the conical and pyramid geometry has taken for the fluid flow analysis using different viscous fluid are investigated. This simulation is useful for analysing the behaviour of the microneedle array, refining its design and enhancing the system performance.

Theortical Analysis

The cross-sectional view of single conical and pyramidal microneedle presented here is displayed in Figure.1a and Figure.1b and it is considered for the structural analysis and microfluidic analysis. H represents the microneedle length, where D_L is the diameter of the hollow cylindrical lumen, L denotes the length of hollow lumen, D_{tip} is the outer diameter of microneedle tip and D_{base} is the base diameter of microneedle.

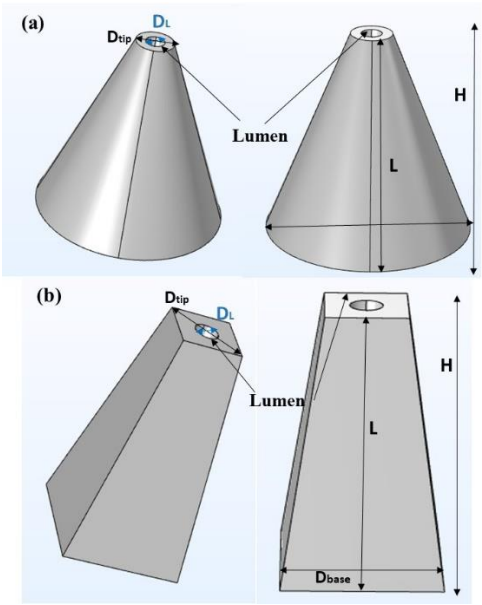

Figure.1 Cross-sectional view of a conical shape b pyramidal shape

Structural Mechanics

To achieve effective microneedle design and anticipate microneedle failure, it is essential to develop a relationship between microneedle geometry and the mechanical properties of the material.

Axial Force

The axial force that the microneedle can endure without breaking is determined by:

$$F_{axial} = \sigma_y A \quad (1)$$

where σ_y is the yield strength of the material and A is the cross-sectional area of the microneedle tip and can be stated as (Bouwstra and Ponec, 2006)

$$A = \pi R^2 \quad (2)$$

Where R is the radius of the microneedle tip.

Buckling Force

The buckling force exerted on the hollow microneedle during insertion is given by (Bodhale, Nisar and Afzulpurkar, 2010)

$$F_{buckling} = \frac{\pi^2 EI}{H^2} \quad (3)$$

where E is young's modulus of the material, I is the moment of inertia of the conical or pyramidal section and H is the length of the microneedle.

Moment of inertia (I) for the conical section is $I = \frac{DH^3}{396}$ and Moment of inertia for pyramidal section is $I = \frac{1}{12}\left({D_o}^4 - {D_i}^4\right)$, where D_o is the outer diameter and D_i is the inner of the hollow pyramidal section.

In order to penetrate the human skin with a microneedle, an external force or pressure must be stronger than the skin's resistance.

Resistive Force

The following equation identifies the skin's resistive force before a skin puncture,

$$F_{resistance} = P_{pierce}\, A \quad (4)$$

Where P_{pierce} is the required pressure to pierce the microneedle into the skin. The needle always penetrates into the skin at a particular angle. A microneedle fracture or break during skin puncture is a serious risk.

Bending Force

The bending force at which the microneedle can withstand without breaking is determined by

$$F_{bending} = \frac{\sigma_y I}{cH} \quad (5)$$

where $c = \frac{D_{base}}{2}$ is the distance from the vertical axis to the outer edge of the section (Aggarwal and Johnston, 2004).

Microfluidic Mechanics

To understand the behaviour of fluid flow within hollow lumen microneedles, microfluidic analysis is very essential. In the case of hollow microneedle, the drug is transported more effectively through the lumen. The microneedle array experiences pressure drop during fluid flow for a variety of reasons, including microneedle shape, array size, fluid viscosity, surface roughness, and microneedle density. There is a significant amount of resistance acting on the microneedle while fluid is passing through it. Measurements and forecasts of fluid mechanics are essential when developing microneedles for transdermal drug delivery so that the microneedles are painless, easily pierce the skin, and large enough to attain the appropriate flow velocity (Tayyaba, Ashraf and Afzulpurkar, 2013).

Poiseulle's law is employed to determine the fluid flow through the microneedle array for the cylindrical lumen

$$Q = \frac{\pi {D_l}^4 (\Delta P)}{128 \mu H} \quad (6)$$

Where Q is the flow rate, D_l is the inner diameter of the hollow lumen, ΔP denotes pressure variation across the microneedle lumen, H denotes the length of the microneedle, and μ is the fluid viscosity.

We may consider an extended Bernoulli equation to model the microneedle geometry as given by

$$\frac{P_{inlet}}{\rho g} + \frac{V_i}{2g} + Z_1 = \frac{P_{outlet}}{pg} + \frac{V_o}{2g} + Z_2 + \frac{fl}{d} + \frac{V^2}{2g} + \sum \frac{KV^2}{2g} \quad (7)$$

Where P_{inlet} is inlet pressure, P_{outlet} is outlet pressure, V_i is inlet fluid velocity, V_o is outlet fluid velocity, f is friction factor, ρ denotes the density of the fluid and K is considered as loss coefficient factor due to inlet and outlets. The output pressure, velocity, and distances (Z_1andZ_2) stay constant because the cylindrical portion is symmetrical about a vertical axis.

The Reynolds number specifies the type of flow, which is expressed as:

$$R_e = \frac{\rho dV}{\mu} \quad (8)$$

If R_e is less than 2100, flow is regarded as laminar otherwise, it is considered to be turbulent.

The friction factor for laminar fluid flow is calculated by

$$f = \frac{64}{R_e} \quad (9)$$

The pressure drop through the microneedles can be calculated from Eq.6:

$$\Delta P = \mu \frac{128QH}{\pi {D_l}^4} + \rho \frac{8Q^2}{\pi^2 {D_l}^2} (K_1 + K_2) \quad (10)$$

Where K_1 and K_2 are the loss coefficient factors due to circular and square edge inlet and outlet.

Simulation Results

Two distinct types of simulations have been performed on a microneedle array using COMSOL Multiphysics, to determine the appropriate microneedle design for drug delivery.The two models of hollow microneedle array are designed: 1. 4x4 conical MN array, 2. 4x4 pyramidal MN array is shown in Figure 2a and 2b. The conical and pyramidal structure of the 4x4 hollow microneedle array was designed for structural analysis in order to examine the mechanical characteristics of the microneedle. The fluid flow rate of 4x4 hollow microneedle array was examined using microfluidic analysis

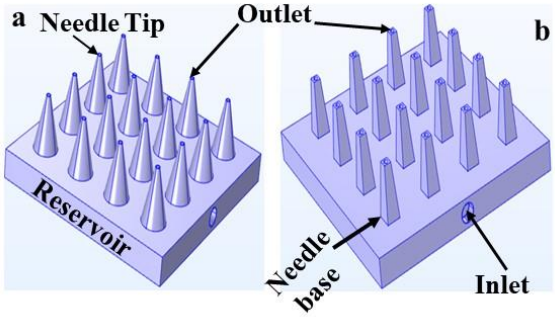

Figure 2. Schematic illustration of proposed three dimensional model in top view a Conical Microneedle array b Pyramidal Microneedle array with reservoir

The performance analysis is made by applying the pressure of 3.18Mpa and the outcome is shown in Figure 3a and 3b. Since the tip of the microneedle experienced a maximum stress of 3.02Mpa (conical), which is less than the yield strength of material, the proposed microneedle can successfully pierce the skin. The simulation output of the axial stress analysis also demonstrates very little tip deflection because of applied pressure at the tip of conical and pyramidal structures.

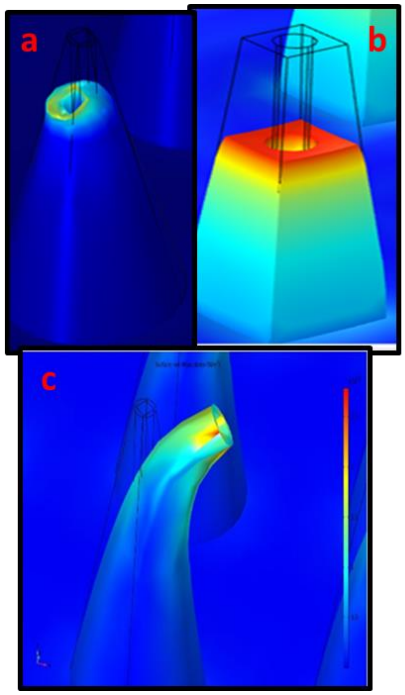

Figure 3. Axial Stress analysis a Conical MN array b Pyramidal MN array c Bending stress analysis of 4x4 pyramidal microneedle array (H=600µm, D_{base}=200µm, D_{tip}=30µm)

In this work, the geometrical structures were subjected to transverse loads to perform bending stress analysis. The transverse force ranges from 0.1 to 2mN is applied to the microneedle tip along the x-axis (Shibata *et al.*, 2007). Equation 4 provides the value for transverse force based on the fracture strength of the material. Figure .3c shows the simulation result for the applied bending force of 0.1788N at the tip. The simulation analysis depicted in Fig.3c revealed that the maximum stress occurs at the microneedle array for the applied bending force, which is less than the yield stress of the material.

For microfluidic analysis, the inlet of the microneedle array was subjected to a pressure ranging from 10 kPa to 100 kPa because these ranges are suggested for various micro pumping devices (Sawon and Samad, 2021).Water and Glucose were considered as working fluids in the fluid domain. The outlet pressure was assumed to be zero (Khumpuang, Maeda and Sugiyama, 2003). The pressure distribution through a 4×4 microneedle array at an applied pressure of 100 kPa is shown in Figure.4. The simulation output demonstrates that pressure and fluid flow distribution are uniform along the microneedle array.

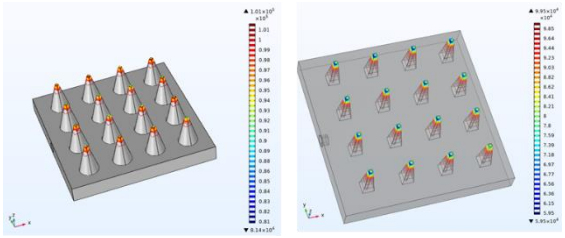

Figure 4. Pressure Distribution for 4 × 4 microneedles array with water as fluid for a Conical Microneedle array and b Pyramidal Microneedle array (H=600µm, D_{base}=200µm, D_{tip}=30µm)

The microneedle array needs a consistent pressure distribution to administer the drug in the correct dosage. The maximum fluid pressure of $1.01e^5$ (conical) and $0.9e^5$ (pyramidal) has been observed through each microneedle. Figure.5 depicts the velocity profile in microfluidic analysis at 100 kPa applied pressure. The velocity of the fluid directly depends on factors such as fluid density, viscosity and area of the lumen. As the designed lumen area is very smaller, the velocity of the fluid increases inside the hollow lumen. The fluid velocity is lesser at the wall area when compared to the lumen core region due to frictional losses.

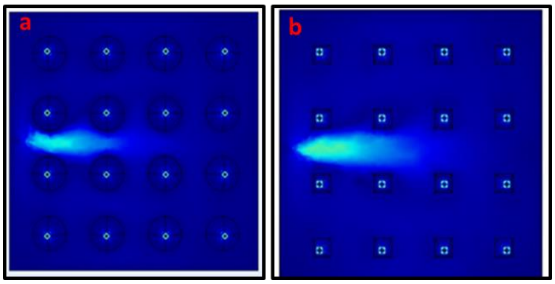

*Figure 5.a Top view of the velocity distribution of fluid in conical microneedle array **b** Top view of velocity profile with the prominent fluid flow across pyramidal microneedle array (H=600µm, D_{base}=200µm, D_{tip}=30µm)*

Figure. 6 depicts the fluid velocity curve of water and glucose with relation to change in inlet pressure. In this graph, the velocity increases with the increase of inlet pressure. Furthermore, it is apparent from the graph that due to its viscosity and density, water has a higher velocity than glucose. It is evident that flow velocity is prominent in the conical MN array when water is the selected fluid. Figure.7 shows the comparison between the flow rates of water as a fluid with variation in applied pressure. The flow rate directly depends on the fluid viscosity, the flow rate is high for a low viscous fluid. Here, the glucose fluid is with higher viscosity of 0.00209 Pa.s (Sawon and Samad, 2021), hence the flow rate of the water is higher when compared to the glucose. The simulation result is shown for a 4x4 conical microneedle and pyramidal MN array with water as a fluid in Fig.13. A higher flow rate of 320µL/min is seen in the conical MN, whereas the pyramidal MN achieves a flow rate of 230µL/min.

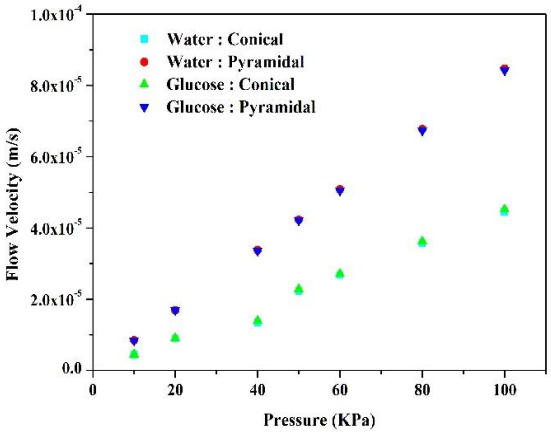

Figure 6.Velocities of different fluids in relation to inlet pressures

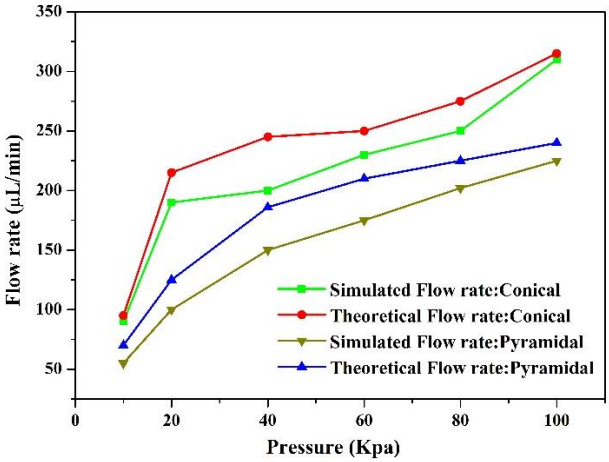

Figure 7. Comparison of theoretical and simulation flow rate of water with variation in applied pressure

Conclusion

A 4x4 hollow PVA microneedle array with centered cylindrical lumen is designed and simulated for the controlled drug delivery system.It is observed that increasing the length of the needle,increases stress with increased chance of instability. The increase in base diameter will decrease the stresses and deflections and enhancing the stability of the structure with increased penetration percentage. The microneedle with larger needle tip diameter induce more pain at injection site. The stress generated proved that the microneedle would remain intact for the applied pressure of 3.16 MPa. It was discovered that a sharp conical tip produces less tension, which leads to painless drug distribution. The fluidic analysis shows that high viscous fluid has lower velocity profile and vice versa. Similarly, the flowrate of water for conical microneedle were 320µL/min and for pyramidal microneedle array were 230µL/min at 100KPa inlet pressure.

References

Aggarwal, P. and Johnston, C. R. (2004) 'Geometrical effects in mechanical characterizing of microneedle for biomedical applications', *Sensors and Actuators, B: Chemical*, 102(2), pp. 226–234. doi: 10.1016/j.snb.2004.04.024.

Bodhale, D. W., Nisar, A. and Afzulpurkar, N. (2010) 'Structural and microfluidic analysis of hollow side-open polymeric microneedles for transdermal drug delivery applications', *Microfluidics and Nanofluidics*, 8(3), pp. 373–392. doi: 10.1007/s10404-009-0467-9.

Bouwstra, J. A. and Ponec, M. (2006) 'The skin barrier in healthy and diseased state', *Biochimica et Biophysica Acta - Biomembranes*, 1758(12), pp. 2080–2095. doi: 10.1016/j.bbamem.2006.06.021.

Griss, P. and Stemme, G. (2002) 'Novel, side opened out-of-plane microneedles for microfluidic transdermal interfacing', *Proceedings of the IEEE Micro Electro Mechanical Systems (MEMS)*, (February), pp. 467–470. doi: 10.1109/memsys.2002.984303.

Ita, K. (2015) 'Transdermal delivery of drugs with microneedles—potential and challenges', *Pharmaceutics*. MDPI AG, 7(3), pp. 90–105. doi: 10.3390/pharmaceutics7030090.

Khumpuang, S., Maeda, R. and Sugiyama, S. (2003) 'Design and fabrication of a coupled microneedle array and insertion guide array for safe penetration through skin', *MHS 2003 - Proceedings of 2003 International Symposium on Micromechatronics and Human Science*, 1, pp. 233–237. doi: 10.1109/MHS.2003.1249938.

Mcallister, D. V, Allen, M. G. and R, M. (2000) 'M Icrofabricated M Icroneedles for G Ene', *Molecules*, pp. 289–313.

Mccrudden, M. T. C. *et al.* (2013) 'Microneedles for intradermal and transdermal delivery', *European Journal of Pharmaceutical Sciences*, 50(5), pp. 623–637. doi: 10.1016/j.ejps.2013.05.005.Microneedles.

Mishra, R., Maiti, T. K. and Bhattacharyya, T. K. (2018) 'Design and scalable fabrication of hollow SU-8 microneedles for transdermal drug delivery', *IEEE Sensors Journal*. IEEE, 18(14), pp. 5635–5644. doi: 10.1109/JSEN.2018.2840335.

Ranamukhaarachchi, S. A. *et al.* (2016) 'Integrated hollow microneedle-optofluidic biosensor for therapeutic drug monitoring in sub-nanoliter volumes', *Scientific Reports*. Nature Publishing Group, 6(July), pp. 1–10. doi: 10.1038/srep29075.

Sawon, M. A. and Samad, M. F. (2021) 'Design and optimization of a microneedle with skin insertion analysis for transdermal drug delivery applications', *Journal of Drug Delivery Science and Technology*. Editions de Sante, 63. doi: 10.1016/j.jddst.2021.102477.

Shibata, T. *et al.* (2007) 'Fabrication and mechanical characterization of microneedle array for cell surgery', *TRANSDUCERS and EUROSENSORS '07 - 4th International Conference on Solid-State Sensors, Actuators and Microsystems*, 3(September), pp. 719–722. doi: 10.1109/SENSOR.2007.4300231.

Tariq, N. *et al.* (2022) 'Numerical Simulation, Analysis, and Fabrication of MEMS-Based Solid Ag and Cu Microneedles for Biomedical Applications', *Mathematical Problems in Engineering*, 2022. doi: 10.1155/2022/1633183.

Tayyaba, S., Ashraf, M. W. and Afzulpurkar, N. (2013) 'Design, simulation, and fabrication of microneedles and a blood filter for use in a hemofiltration system', *IEEE Transactions on Automation Science and Engineering*. IEEE, 10(2), pp. 252–266. doi: 10.1109/TASE.2012.2230166.

Wang, P. C. *et al.* (2009) 'Hollow polymer microneedle array fabricated by photolithography process combined with micromolding technique', *Proceedings of the 31st Annual International Conference of the IEEE Engineering in Medicine and Biology Society: Engineering the Future of Biomedicine, EMBC 2009*, pp. 7026–7029. doi: 10.1109/IEMBS.2009.5333317.

Yan, Q. *et al.* (2022) 'The Finite Element Analysis Research on Microneedle Design Strategy and Transdermal Drug Delivery System', *Pharmaceutics*, 14(8), p. 1625. doi: 10.3390/pharmaceutics14081625.

Acknowledgements

This work was supported in part by the Department of Science and Technology under Grant TDP/BDTD/23/2019. The authors thank Indian Science Technology and Engineering facilities Map (I-STEM), a program supported by Office of the Principal Scientific Adviser to the Govt. of India, for enabling access to the COMSOL Multiphysics software suite used to carry out this work.